Supplementary Material for:
Monolayer Spontaneous Curvature of Raft-Forming Membrane Lipids

Benjamin Kollmitzer, Peter Heftberger, Michael Rappolt, and Georg Pabst

September 23, 2013, Graz

S1 Electron density calculation

All recognizable peaks of the intensity $I(q)$ were individually fitted using least-squares plus a linear background estimator, yielding peak intensities $I_{h,k}$ and positions $q_{h,k}$. The (1,1) and (2,0) peaks are close and were fitted together with a common linear background (Fig. S1).
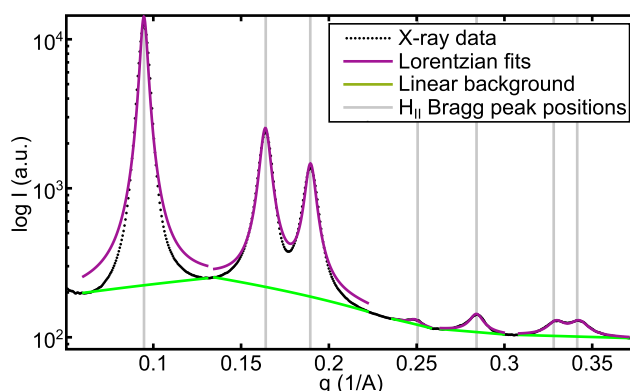

Figure S1: Analysis of DOPE at 35 °C.

We followed the procedure described by Rappolt et al.[1] for calculating electron maps. The lattice parameter a was determined via the reflection law $\sqrt{3}\,a\,q_{h,k}/4\pi = 1, \sqrt{3}, 2, \sqrt{7}, \ldots$. Fourier synthesis yielded the electron density in real-space

$$\rho(\vec{r}) = \sum_{h,k} \alpha_{h,k} \sqrt{\frac{I_{h,k}\, q_{h,k}^2}{m_{h,k}}} \cdot \cos\left(2\pi\, \vec{q}_{h,k} \cdot \vec{r}\right), \tag{S1}$$

where multiplication of the intensity with $q_{h,k}^2$ is known as Lorentz correction[2], $m_{h,k}$ is the multiplicity of the equivalent diffraction planes (6 for $(1,0),(1,1),(3,0)\ldots$; 12 for $(2,1),(3,1),(3,2)\ldots$)

S1

and $\alpha_{h,k}$ is the phase (± 1 for centrosymmetric structures as in this work). Literature[3–5] suggests $(+--+++++-)$ as phasing condition for DOPE-rich, fully hydrated H_{II} phases. Figure S2 gives an example for a calculated electron density map. Other phase combinations were tested, but yielded electron densities incompatible with the known structure.
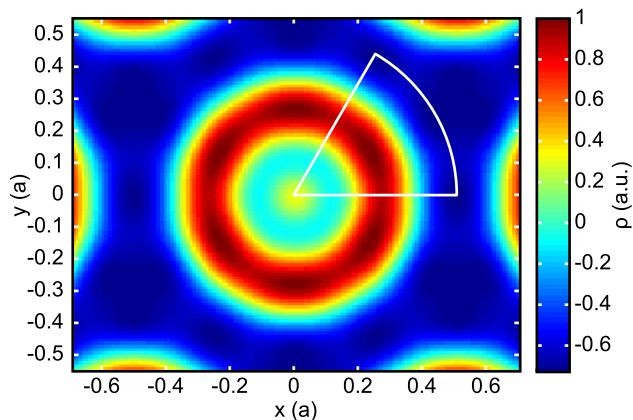

Figure S2: 2D electron density map $\rho(x,y)$ for DOPE at $35\,^{\circ}C$. The white circular segment indicates the region, where the radial cross sections of ρ are evaluated for the location of the pivotal plane. Coordinates are normalized by the unit cell parameter a.

A Gaussian fit to the radial cross section of the electron density yielded position R_p and width σ_p of the headgroup (Fig. S3). We averaged these quantities over azimuthal angles ranging from $0°$ (x-axis) to $60°$, as indicated by the circular segment in Fig. S2.
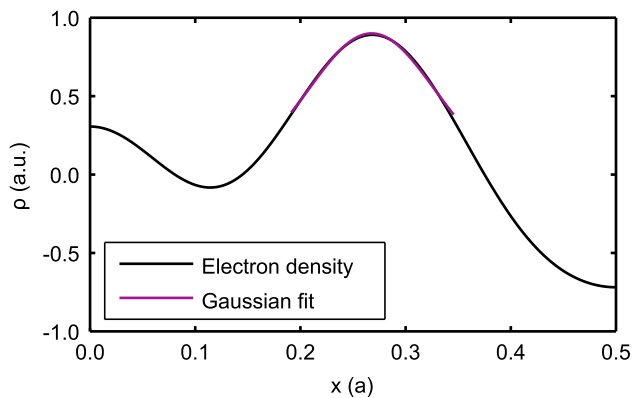

Figure S3: Radial cross section of the electron density from Fig. S2 along the x-axis with Gaussian fit for the headgroup region.

S2 Tieline parameterization

For parameterizing coexistence regions and tieline fields, we applied the method described in[6,7]. Ternary phase diagram coordinates (x, y, z) with $x + y + z = 1$ and $\{x, y, z\} \in [0, 1]$ are transformed into a two-dimensional vector $\vec{\Psi} = (\xi, \eta)$ with components $\xi = z\sqrt{3}/2$ and $\eta = y + z/2$. Bézier curves

$$\vec{B}(t) = \sum_{l=0}^{n} \binom{n}{l} (1-t)^{n-l} t^l \vec{P}_l \tag{S2}$$

of degree $n = 5$ were reported to describe phase boundaries well in the (ξ, η)-space. To relate these curves to the tieline fields, Smith and coworkers[6] introduced the relationships

$$t_{Lo}(u) = \tau_c + (1 - \tau_c) u \tag{S3}$$

$$t_{Ld}(u) = \tau_c - \frac{\tau_c u}{u + c(1-u)}, \tag{S4}$$

where τ_c characterizes the critical point and c takes care of tieline fanning. Equations (S3) and (S4) allow to express the tieline endpoint compositions in 2D as $\vec{\Psi}_{Lo}(u) = \vec{B}(t_{Lo}(u))$ and $\vec{\Psi}_{Ld}(u) = \vec{B}(t_{Ld}(u))$, where $\vec{\Psi}_{Lo}(0) = \vec{\Psi}_{Ld}(0)$ describes the critical point.

    We determined the 6 control points $\{\vec{P}_l\}$ from a least squares fit of the Bézier curves to the boundary coordinates of previously published compositional phase diagrams[7–9]. The fitting was performed with the MATLAB® function grad7.m listed in[10]. Having determined the control points, we calculated τ_c, by minimizing the distance from the critical point to $\vec{B}(\tau_c)$. Analogously, the auxiliary points $\{\tau_{Lo,i}, \tau_{Ld,i}\}$ were computed by minimizing the distance from $\vec{B}(\tau_{Lo/d,i})$ to the intersection of the i-th tieline with the phase boundary on the L_o/L_d side. The parameter c describing the tieline fanning was calculated by solving

$$c = \frac{(\tau_{Lo,i} - \tau_c)\, \tau_{Ld,i}}{(\tau_{Ld,i} - \tau_c)(\tau_{Lo,i} - 1)} \tag{S5}$$

in the least squares sense. Equation (S5) follows directly from eliminating u in Eqs. (S3) and (S4). The resulting parameters describing the reported tielines from[7–9] are listed in Tab. S1.

S3 Line tension calculations

Based on elastic deformations of monolayers, Kuzmin et al.[11] derived an expression for the line tension γ between two coexisting phases L_o and L_d

$$\gamma = \frac{1}{Z}\sqrt{B_d K_d B_o K_o}\,\frac{\delta^2}{h_0^2} - \frac{1}{2Z}\left(J_{0,d} B_d - J_{0,o} B_o\right)^2, \tag{S6}$$

with $Z = \sqrt{B_d K_d} + \sqrt{B_o K_o}$, monolayer bending moduli B, tilt moduli K, monolayer spontaneous curvatures J_0, and structural parameters $\delta = h_o - h_d$ and $h_0 = (h_o + h_d)/2$ relating the positions h of the monolayer neutral planes. We refer to the first term of Eq. (S6) as elastic γ_{el} and to the second as curvature contribution γ_{J0} to the line tension. It was already pointed out in 4.2, that

Table S1: Parameters describing the tieline fields of published phase diagrams.

	DOPC/DPPC/Chol[§]	POPC/eggSM/Chol[¶]	DOPC/DSPC/Chol[‖]
$\vec{P}_0$	(0.268, 0.568)	(0.438, 0.087)	(0.155, 0.074)
$\vec{P}_1$	(0.204, 0.174)	(0.112, 0.029)	(0.176, 0.265)
$\vec{P}_2$	(0.361, 0.252)	(0.531, 0.510)	(0.300, 0.380)
$\vec{P}_3$	(0.603, 0.554)	(0.468, 0.126)	(0.624, 0.365)
$\vec{P}_4$	(0.778, 0.196)	(0.671, 0.320)	(0.646, 0.391)
$\vec{P}_5$	(0.780, 0.189)	(0.718, 0.208)	(0.764, 0.224)
τ_c	0.429	0.297	0.506
c	1.115	0.832	1.000

[§] Phase diagram from [8]
[¶] Phase diagram from [9]
[‖] Values taken from [7], fits yielded similar results

these relations hold for $|J_0|$ much smaller than $1/h$. In the following examples, we therefore verify that $|J_0| \cdot h < 1$.

We calculate the spontaneous curvatures $J_{0,d}$ and $J_{0,o}$ according to Eq. (4) using known compositions of L_o and L_d. The moduli in Eq. (S6) are effective moduli of the domains and normalized by cross-sectional area. Per-lipid tilt moduli κ_j reported in [14] were taken, normalized by the lipid areas and averaged over the corresponding phase. Averaging was achieved by defining for each phase an average lipid, of volume $\bar{V} = \sum_j \chi_j V_j$ and area $\bar{A} = \bar{V}/h$, where V_j is the volume of constituent lipid j and h the monolayer thickness of a given domain. We further assumed that the effective tilt modulus can be expressed as $K = \sum_j \chi_j \kappa_j / \bar{A}$.

Lipid volumes needed in this section are available in the literature: [12,13]

	DOPC	POPC	DPPC	DSPC	Chol
V (nm^3)	1.30	1.26	1.23	1.35	0.63

Example 1: Ternary mixtures

All parameters used for calculations are listed in Tab. S2. The magnitude of the spontaneous curvature J_0 is at least by a factor of 2 smaller than the monolayer thickness, meaning that the use of Eq. (S6) is justified. The resulting line tensions obtained by Eq. (S6) are reported in Tab. S3.

Example 2: Varying domain sizes

For the quaternary mixture DOPC/POPC/DSPC/Chol, a similar calculation has already been used to rationalize the domain size behavior as a function of $\rho = \chi_{DOPC}/(\chi_{DOPC} + \chi_{POPC})$. [15] It was found, that the nanoscopic domains in POPC/DSPC/Chol grew bigger by replacing POPC with DOPC, until finally microscopic domains for DOPC/DSPC/Chol were detected. We repeat

Table S2: Compositions χ, temperatures T, and elastic and structural parameters for Example 1.

	DOPC/DPPC/Chol		DOPC/DSPC/Chol	
	L_d	L_o	L_d	L_o
$\chi_1 : \chi_2 : \chi_3$	0.66:0.19:0.15	0.12:0.58:0.30	0.74:0.09:0.17	0.12:0.56:0.32
T (°C)	15	15	22	22
B (kT) [*]	17±2	49±3	15±1	53±4
κ_1 (kT) [*]	11±1	34±3	9±1	44±3
κ_2 (kT) [*]	14±1	53±3	10±1	60±4
κ_3 (kT) [*]	15±1	48±3	15±2	49±2
h (nm) [*,†]	1.5	1.8	1.5	2.0
$\bar{V}$ (nm^3)	1.2	1.1	1.2	1.1
$\bar{A}$ (nm^2)	0.77	0.58	0.80	0.57
K (kT nm^{-2})	15	85	13	97
J_0 (nm^{-1})	-0.08	-0.05	-0.14	-0.21
$|J_0| \cdot h$	0.13	0.22	0.10	0.42

[*] Taken from [14]

[†] Although the thickness was not reported explicitly, it was used in the SAXS evaluation of [14]

Table S3: Resulting line tensions γ, and elastic γ_{el} and curvature contributions γ_{J0} for Example 1.

	DOPC/DPPC/Chol	DOPC/DSPC/Chol
γ_{el} (pN)	1.4	3.4
γ_{J0} (pN)	0.0	-1.8
γ (pN)	1.4	1.6

Table S4: Bilayer thickness t and spontaneous curvature J_0 for Example 2.

ρ (%)	0	5	10	17	20	35	100
t_{Ld} (nm) [‡]	3.84	3.80	3.80	3.76	3.77	3.67	3.51
t_{Lo} (nm) [‡]	4.48	4.48	4.48	4.46	4.46	4.46	4.48
$J_{0,Ld}$ (nm^{-1})	-0.06	-0.06	-0.06	-0.07	-0.07	-0.08	-0.12
$J_{0,Lo}$ (nm^{-1})	-0.16	-0.16	-0.17	-0.17	-0.17	-0.18	-0.19
$|J_{0,Ld}| \cdot h_{Ld}$	0.09	0.10	0.10	0.11	0.11	0.12	0.18
$|J_{0,Lo}| \cdot h_{Lo}$	0.30	0.31	0.32	0.32	0.33	0.34	0.38

[‡] Taken from [15]

Table S5: Domain radii R and resulting line tensions γ with elastic γ_{el} and curvature contributions γ_{J0} for Example 2.

ρ (%)	0	5	10	17	20	35	100
R (nm) [‡]	68	85	98	111	124	162	>225
γ_{el} (pN)	1.7	1.9	1.9	2.1	2.0	2.7	4.1
γ_{J0} (pN)	-0.6	-0.6	-0.6	-0.6	-0.6	-0.7	-0.7
γ (pN)	1.1	1.4	1.3	1.4	1.4	2	3.4

[‡] Taken from [15]

that calculation, but with better determined values for bending moduli, tilt moduli and spontaneous curvature.

The compositions for DOPC/DSPC/Chol from Example 1 are similar to the compositions for $\rho = 1$. We use therefore these MD results[14] also for the current example. We further assume the per-lipid tilt moduli of POPC and DOPC to be equal. This means, that the results for $\rho = 1$ should be reliable, but become more imprecise with increasing POPC content. Bilayer thickness t informations are taken from[15]. To obtain the height of the neutral plane h, which should be close to the apolar/polar interface[16], we subtract 0.3 nm from the monolayer thickness. This value is a reasonable guess for the distance between the Luzzatti position and the apolar/polar interface.[12] The applied bilayer thicknesses and monolayer spontaneous curvatures are listed in Tab. S4. Equation (S6) yields with these values the line tensions given in Tab. S5. Results are shown in Fig. 6. The magnitude of the spontaneous curvature J_0 is at least by a factor of 2 smaller than the monolayer thickness, meaning that the use of Eq. (S6) is justified.

S4 Spontaneous curvature extrapolation

The dependence of $J_0^{mix}(T, \chi)$ on temperature T and concentration χ is given in Tabs. S6–S12 and plotted in Figs. S4–S10. In the figures, black crosses depict valid data points used for extrapolation, while green data points were not considered because there $\chi > \chi_{crit}$.

Table S6: Spontaneous curvature J_0^{mix} as function of temperature T [°C] and concentration χ [mol%] Chol in DOPE. Numbers above χ_{crit} are untrustworthy

	10 mol%	20 mol%	30 mol%	40 mol%	50 mol%	χ_{crit} (mol%)
15 °C	−0.38	−0.39	−0.39	−0.39	−0.39	> 40
25 °C	−0.40	−0.40	−0.41	−0.41	−0.41	> 40
35 °C	−0.41	−0.42	−0.43	−0.44	−0.45	> 40
45 °C	−0.43	−0.44	−0.45	−0.46	−0.47	> 40
55 °C	−0.44	−0.45	−0.46	−0.48	−0.50	> 50

Table S7: Spontaneous curvature J_0^{mix} as function of temperature T [°C] and concentration χ [mol%] DOPC in DOPE. Numbers above χ_{crit} and NaN are untrustworthy

	10 mol%	20 mol%	30 mol%	40 mol%	50 mol%	χ_{crit} (mol%)
15 °C	−0.34	−0.30	NaN	−0.24	−0.22	> 50
25 °C	−0.35	−0.31	NaN	−0.26	−0.23	> 50
35 °C	−0.36	−0.33	NaN	−0.27	−0.25	> 50
45 °C	−0.38	−0.34	NaN	−0.29	−0.26	> 50
55 °C	−0.39	−0.36	NaN	−0.30	−0.27	> 50

Table S8: Spontaneous curvature J_0^{mix} as function of temperature T [°C] and concentration χ [mol%] DPPC in DOPE. Numbers above χ_{crit} are untrustworthy

	10 mol%	20 mol%	30 mol%	40 mol%	50 mol%	χ_{crit} (mol%)
15 °C	−0.32	−0.30	−0.31	−0.31	−0.33	> 10
25 °C	−0.33	−0.29	−0.26	−0.25	−0.28	> 20
35 °C	−0.35	−0.31	−0.27	−0.24	−0.41	> 20
45 °C	−0.37	−0.32	−0.28	−0.25	−0.24	> 30
55 °C	−0.39	−0.34	−0.30	−0.28	−0.25	> 30

Table S9: Spontaneous curvature J_0^{mix} as function of temperature T [°C] and concentration χ [mol%] DSPC in DOPE. Numbers above χ_{crit} and NaN are untrustworthy

	10 mol%	20 mol%	30 mol%	40 mol%	50 mol%	χ_{crit} (mol%)
15 °C	−0.35	−0.35	−0.35	−0.35	NaN	> 10
25 °C	−0.35	−0.34	−0.35	−0.36	NaN	> 10
35 °C	−0.36	−0.34	−0.34	NaN	NaN	> 20
45 °C	−0.37	−0.35	−0.35	−0.37	NaN	> 20
55 °C	−0.39	−0.36	−0.34	−0.34	−0.27	> 20

Table S10: Spontaneous curvature J_0^{mix} as function of temperature $T\,[°C]$ and concentration $\chi\,[mol\%]$ POPC in DOPE. Numbers above χ_{crit} and NaN are untrustworthy

	10 mol%	20 mol%	30 mol%	40 mol%	50 mol%	$\chi_{crit}\,(mol\%)$
15 °C	−0.33	−0.29	−0.25	−0.22	NaN	> 40
25 °C	−0.34	−0.31	−0.26	−0.24	NaN	> 40
35 °C	−0.36	−0.32	−0.28	−0.25	−0.22	> 40
45 °C	−0.37	−0.33	−0.29	−0.27	−0.23	> 50
55 °C	−0.38	−0.34	−0.30	−0.27	−0.24	> 50

Table S11: Spontaneous curvature J_0^{mix} as function of temperature $T\,[°C]$ and concentration $\chi\,[mol\%]$ SOPC in DOPE. Numbers above χ_{crit} and NaN are untrustworthy

	10 mol%	20 mol%	30 mol%	40 mol%	50 mol%	$\chi_{crit}\,(mol\%)$
15 °C	−0.32	−0.28	−0.25	−0.22	−0.19	> 30
25 °C	−0.34	−0.30	−0.27	−0.23	NaN	> 30
35 °C	−0.35	−0.31	−0.28	−0.25	−0.22	> 30
45 °C	−0.37	−0.33	−0.30	−0.27	−0.22	> 30
55 °C	−0.39	−0.34	−0.31	−0.28	−0.24	> 30

Table S12: Spontaneous curvature J_0^{mix} as function of temperature $T\,[°C]$ and concentration $\chi\,[mol\%]$ eggSM in DOPE. Numbers above χ_{crit} and NaN are untrustworthy

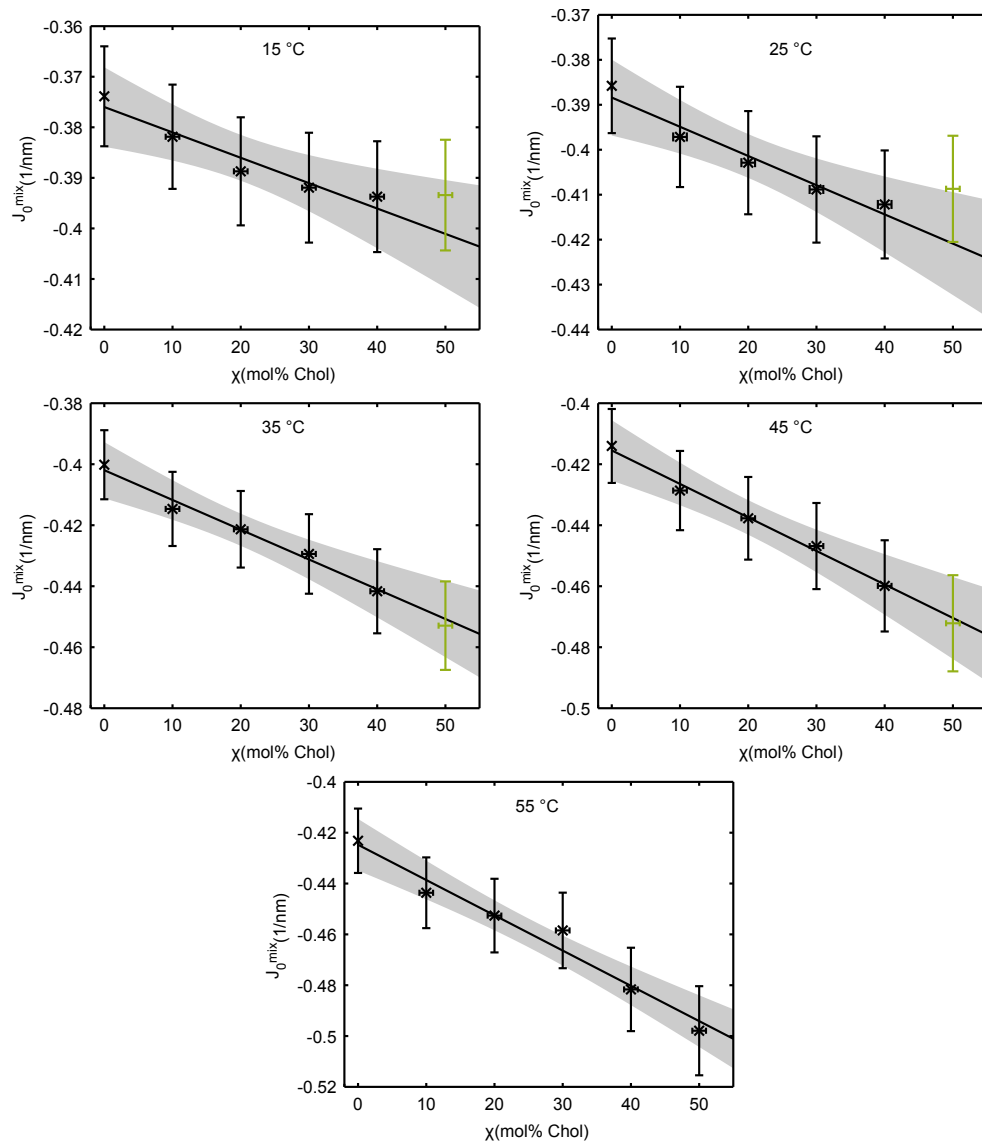|	10 mol%	20 mol%	30 mol%	40 mol%	50 mol%	$\chi_{crit}\,(mol\%)$
15 °C	−0.35	−0.28	−0.29	NaN	NaN	> 10
25 °C	−0.37	−0.35	−0.28	NaN	NaN	> 10
35 °C	−0.38	−0.36	−0.30	NaN	NaN	> 10
45 °C	−0.39	−0.38	−0.30	NaN	NaN	> 10
55 °C	−0.39	−0.39	−0.33	NaN	NaN	> 10

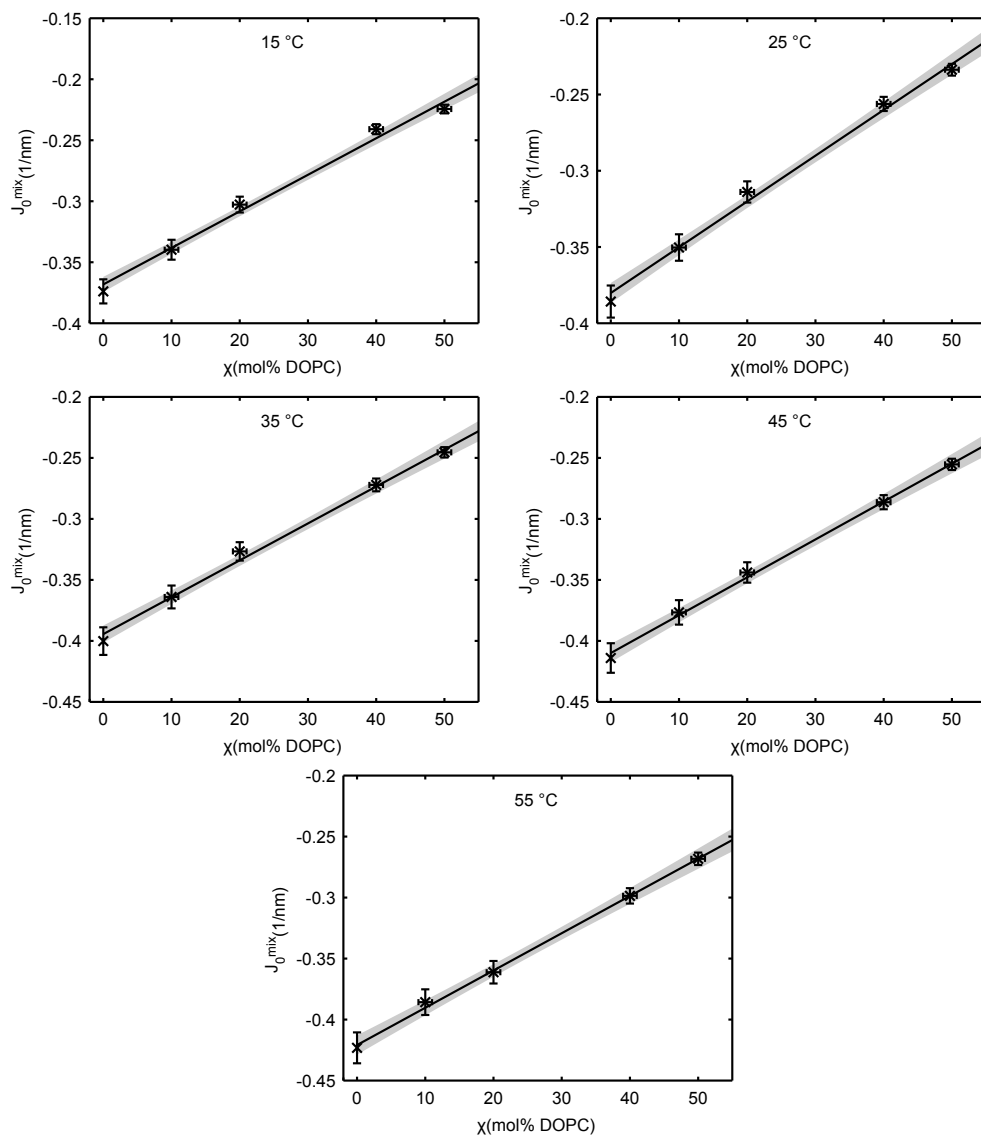Figure S4: Determination of J_0 for Chol.
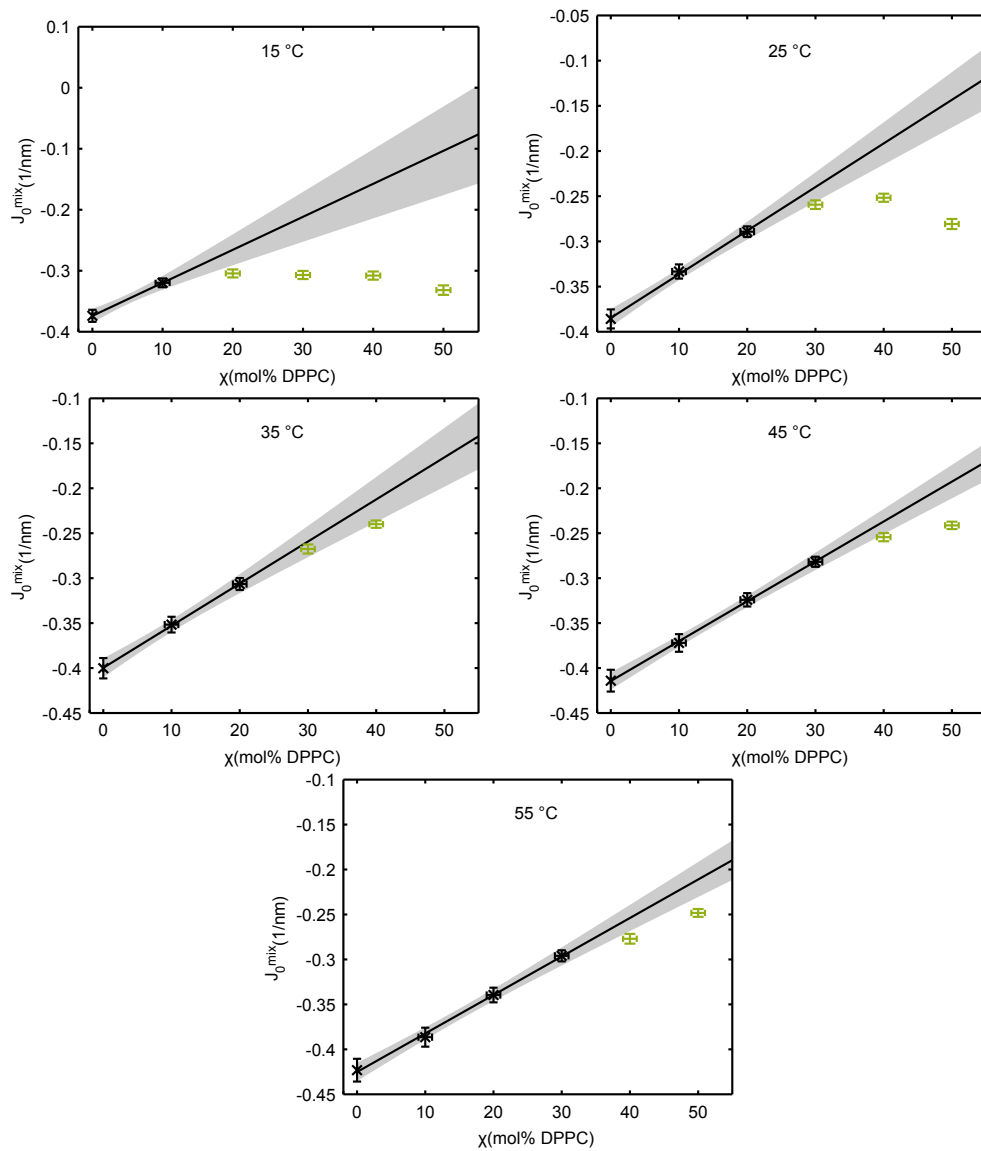
Figure S5: Determination of J_0 for DOPC.

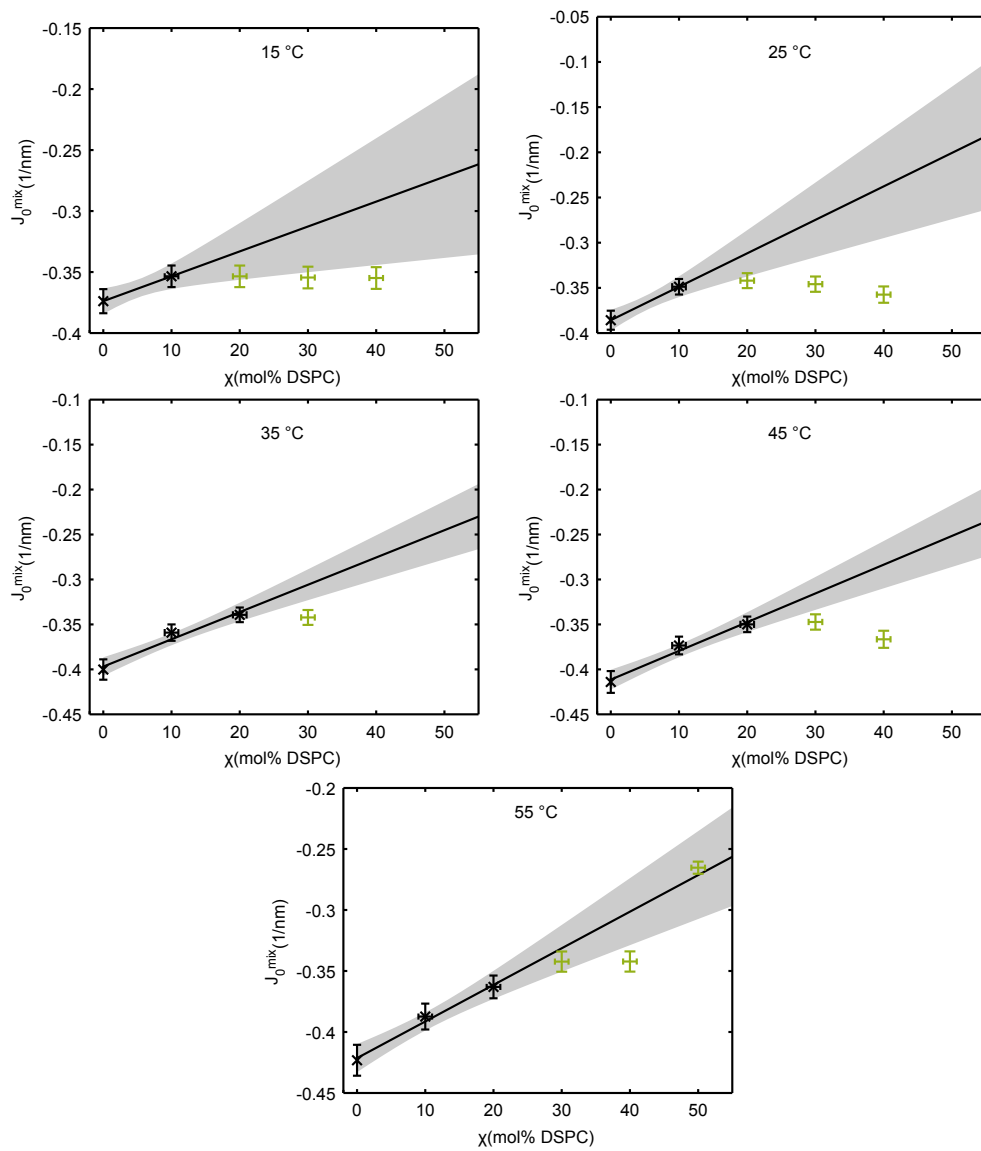Figure S6: Determination of J_0 for DPPC.
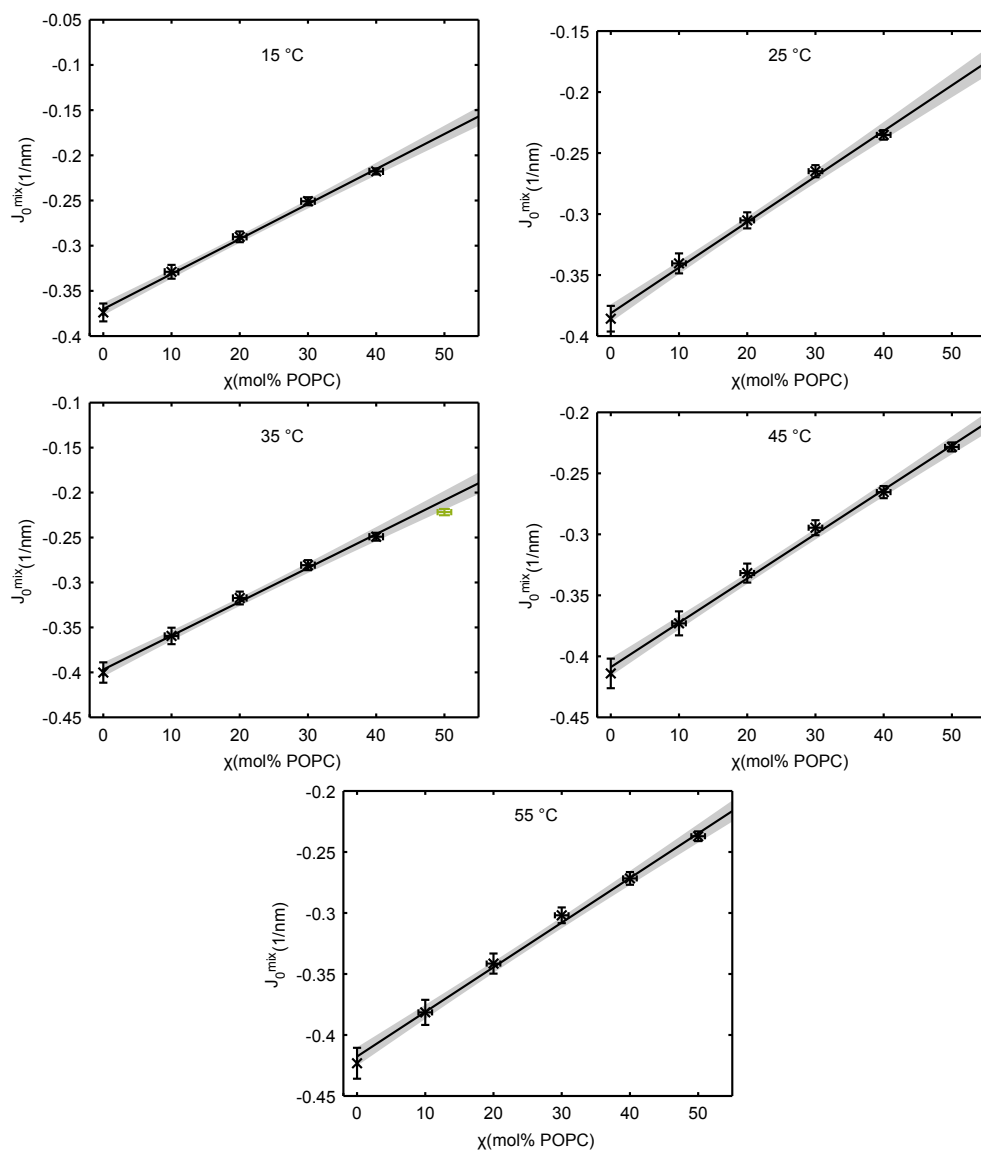
Figure S7: Determination of J_0 for DSPC.

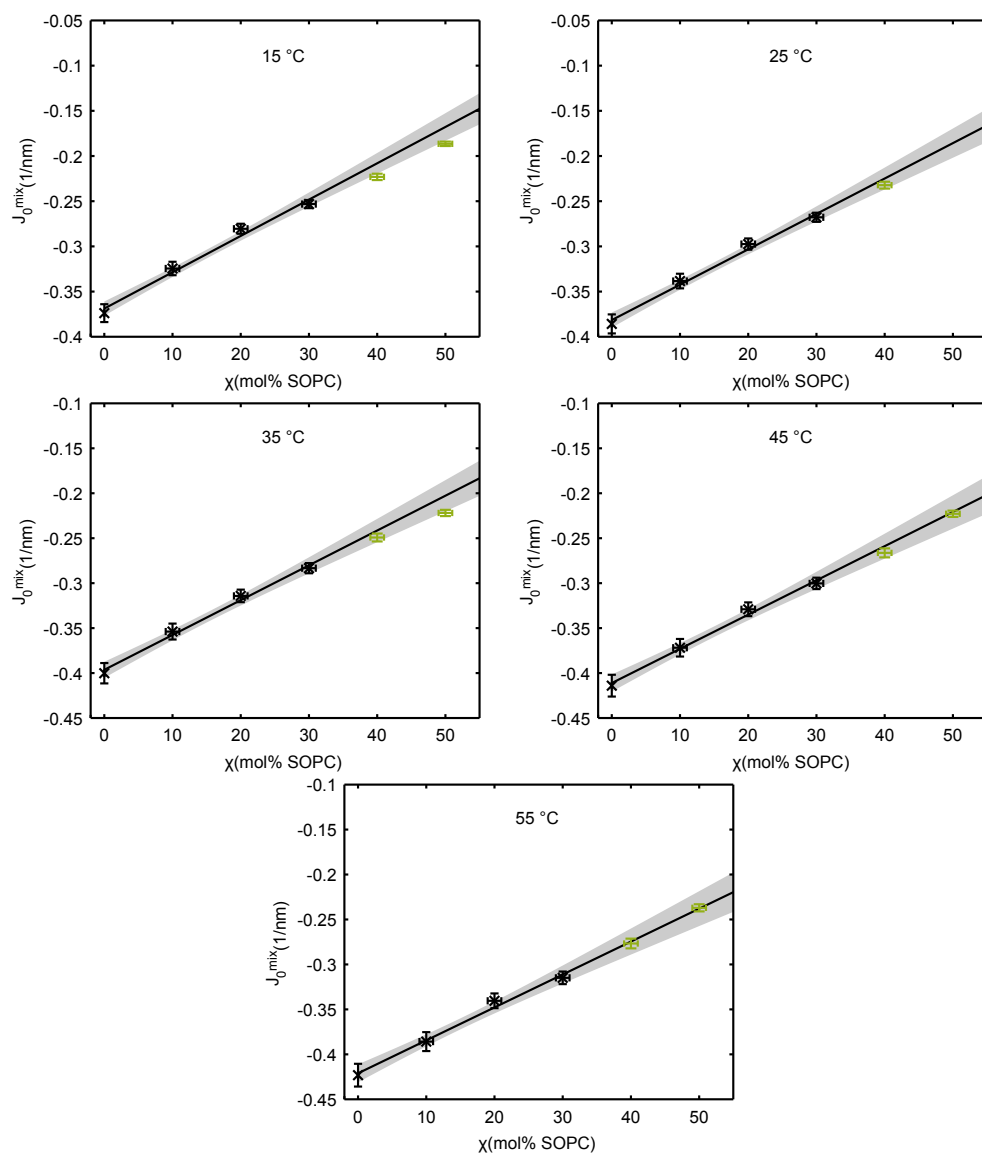Figure S8: Determination of J_0 for POPC.
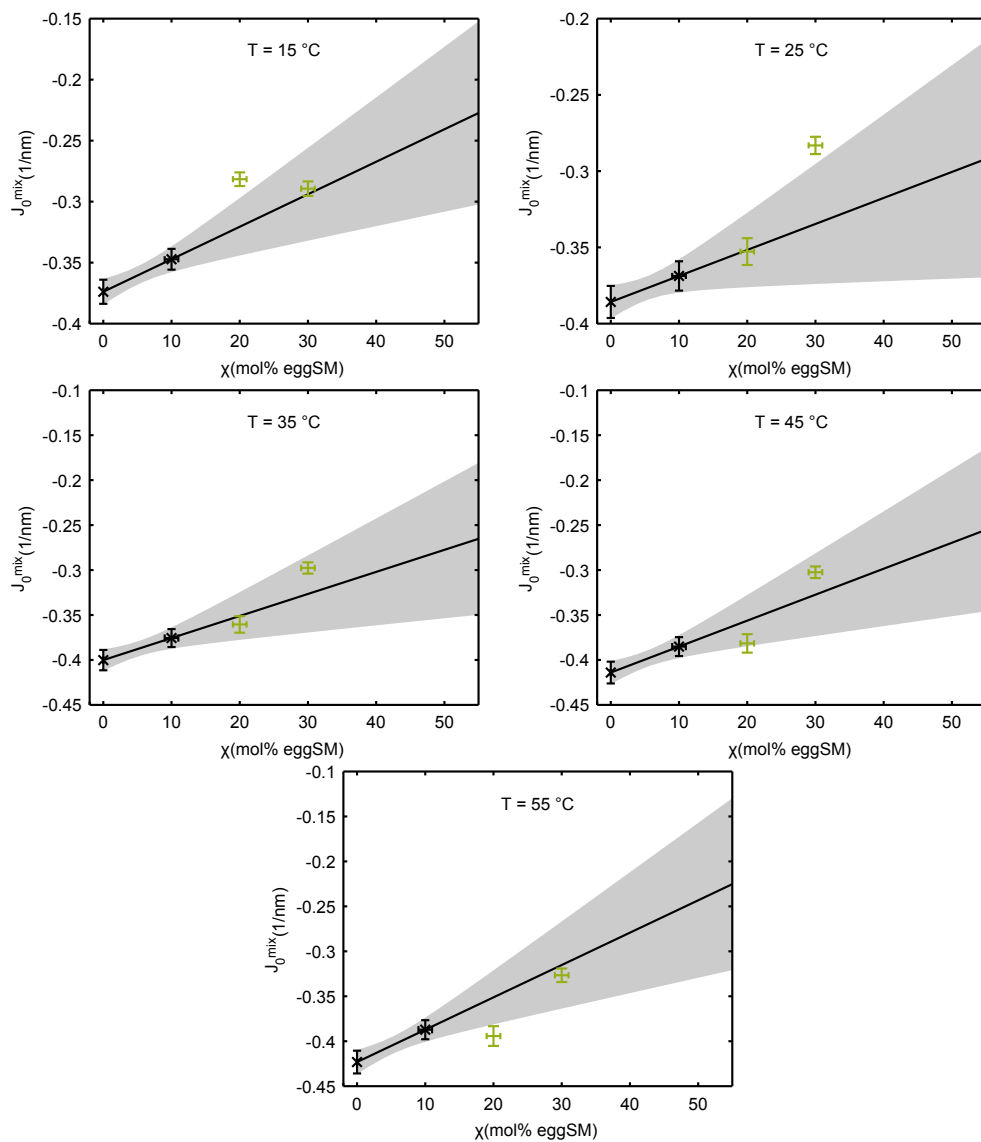
Figure S9: Determination of J_0 for SOPC.
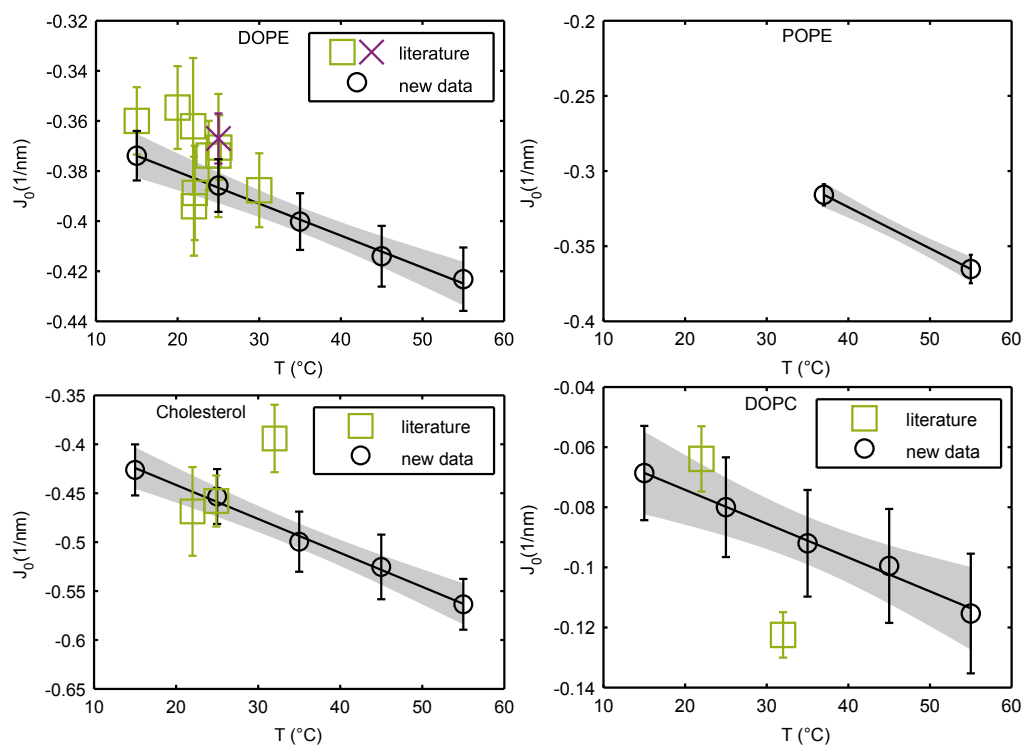
Figure S10: Determination of J_0 for eggSM.

Figure S11: Temperature dependence of $J_0(T)$ compared with literature data.[16–24]

S5 Temperature dependence of spontaneous curvature

Each lipid's spontaneous curvature $J_0(T)$ as a function of temperature T is presented in Figs. S11–S12 (black circles) in comparison with literature data determined at the pivotal plane* (green squares) and the neutral plane (violet crosses). The black straight line is the result of the linear fit according to Eq. (2), while the gray band depicts its error via Eq. (3).

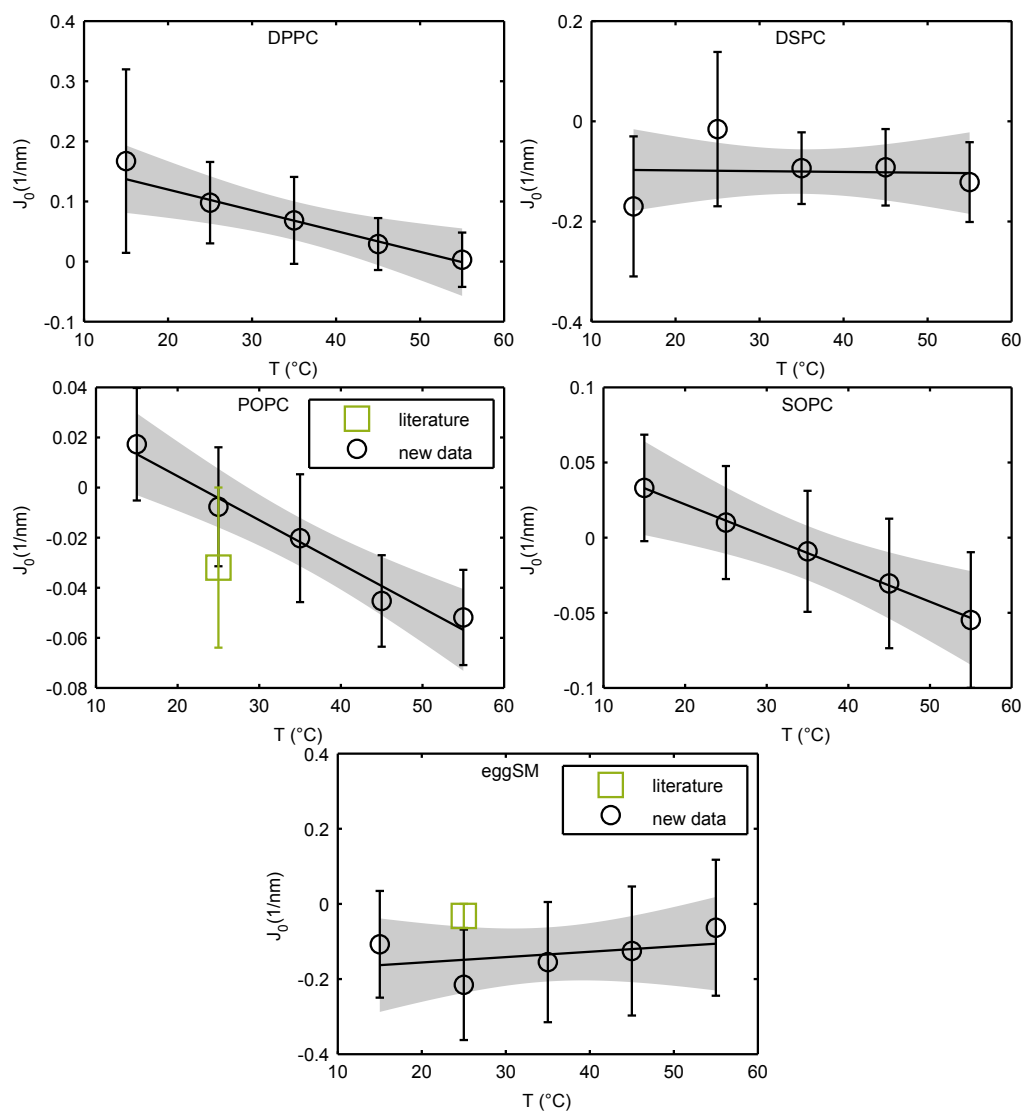*Similar to Fig. 3, we rescaled reported values to $J_0 \sim J_{0p}(1+\beta)$, with $\beta = 0.065 \pm 0.035$ determined in [17].

Figure S12: Temperature dependence of $J_0(T)$ compared with literature data. [22]

References

[1] M. Rappolt, A. Hickel, F. Bringezu and K. Lohner, *Biophys. J.*, 2003, **84**, 3111–3122.

[2] B. E. Warren, *X-ray diffraction*, Addison-Wesley Pub. Co., Reading, Mass., 1969.

[3] D. C. Turner and S. M. Gruner, *Biochemistry*, 1992, **31**, 1340–1355.

[4] P. E. Harper, D. A. Mannock, R. N. Lewis, R. N. McElhaney and S. M. Gruner, *Biophys. J.*, 2001, **81**, 2693–2706.

[5] M. Rappolt, A. Hodzic, B. Sartori, M. Ollivon and P. Laggner, *Chem. Phys. Lipids*, 2008, **154**, 46–55.

[6] A. K. Smith and J. H. Freed, *J. Phys. Chem. B*, 2009, **113**, 3957–3971.

[7] F. A. Heberle, J. Wu, S. L. Goh, R. S. Petruzielo and G. W. Feigenson, *Biophys. J.*, 2010, **99**, 3309–3318.

[8] P. Uppamoochikkal, S. Tristram-Nagle and J. F. Nagle, *Langmuir*, 2010, **26**, 17363–17368.

[9] I. V. Ionova, V. A. Livshits and D. Marsh, *Biophys. J.*, 2012, **102**, 1856–1865.

[10] T. A. Pastva, *Master's thesis*, Naval Postgraduate School, Monterey, California, 1998.

[11] P. I. Kuzmin, S. A. Akimov, Y. A. Chizmadzhev, J. Zimmerberg and F. S. Cohen, *Biophys. J.*, 2005, **88**, 1120–1133.

[12] N. Kučerka, M.-P. Nieh and J. Katsaras, *Biochim. Biophys. Acta, Biomembr.*, 2011, **1808**, 2761–2771.

[13] A. I. Greenwood, S. Tristram-Nagle and J. F. Nagle, *Chem. Phys. Lipids*, 2006, **143**, 1–10.

[14] G. Khelashvili, B. Kollmitzer, P. Heftberger, G. Pabst and D. Harries, *J. Chem. Theory Comput.*, 2013.

[15] F. A. Heberle, R. S. Petruzielo, J. Pan, P. Drazba, N. Kučerka, R. F. Standaert, G. W. Feigenson and J. Katsaras, *J. Am. Chem. Soc.*, 2013, **135**, 6853–6859.

[16] R. P. Rand and N. L. Fuller, *Biophys. J.*, 1994, **66**, 2127–2138.

[17] S. Leikin, M. M. Kozlov, N. L. Fuller and R. P. Rand, *Biophys. J.*, 1996, **71**, 2623–2632.

[18] E. E. Kooijman, V. Chupin, N. L. Fuller, M. M. Kozlov, B. de Kruijff, K. N. J. Burger and R. P. Rand, *Biochemistry*, 2005, **44**, 2097–2102.

[19] N. Fuller, C. R. Benatti and R. P. Rand, *Biophys. J.*, 2003, **85**, 1667–1674.

[20] Z. Chen and R. P. Rand, *Biophys. J.*, 1997, **73**, 267–276.

[21] M. M. Kozlov, S. Leikin and R. P. Rand, *Biophys. J.*, 1994, **67**, 1603–1611.

[22] B. Boulgaropoulos, M. Rappolt, B. Sartori, H. Amenitsch and G. Pabst, *Biophys. J.*, 2012, **102**, 2031–2038.

[23] J. A. Szule, N. L. Fuller and R. P. Rand, *Biophys. J.*, 2002, **83**, 977–984.

[24] R. P. Rand, N. L. Fuller, S. M. Gruner and V. A. Parsegian, *Biochemistry*, 1990, **29**, 76–87.